bearings as a simple granular material (Cui and O'Sullivan, 2006; O'Sullivan, 2011; Bernhardt et al. 2016) and have obtained good agreement between the laboratory and DEM responses. In addition to the different boundaries used in the laboratory direct shear testing, DEM simulations often use a fixed-particle boundary or a sawtooth boundary to simplify the model and reduce computational cost. For the fixed-particle boundary, the rough boundary is created in the laboratory sample by physically attaching particles to the boundary plates, and it can be simulated in the numerical models by fixing the velocities and rotations of the particles in contact with the top and bottom boundaries. Currently, there is insufficient information available regarding how these types of boundaries would also perform in the laboratory experiments.

As discussed, according to ASTM D3080, exact criteria for the texture of the inserts have not been established. Therefore, the current study focuses on four different types of commonly used boundaries for direct shear testing. The results from tests conducted on steel ball bearings are presented here and will also be used for experimental validation of DEM simulations in future studies.

DIRECT SHEAR EXPERIMENTS

The direct shear apparatus used in the current study consisted of the typical two-part box which encased a cylindrical sample of 63.5 mm in diameter and a height of 46.0 mm. The bottom half of the shear box was moved at a constant rate of 0.508 mm/min in accordance with ASTM D3080, while the top half was held stationary in the horizontal direction. Four different types of boundaries were proposed in this study. The geometry, dimensions, and spacing of the four boundaries are presented in Figure 1. The boundary plates were created using a gypsum based 3D printer. 3D printing the plates allowed for the rapid generation of different geometries without the need for machining the boundary plates. The ratio (R) of the spacing of the projections on the grid insert to the maximum diameter of the particle for the first two grid inserts chosen were 1.5 and 4.8, as shown in Figure 1a and 1b, respectively. The saw tooth boundaries (Figure 1c) were modeled such that the base of one triangular tooth and height to the vertex were 3mm and 1.5mm respectively. For the fixed-particle boundary (Figure 1d), ball bearings were glued to a flat 3D printed plate and used in the experiment instead of grid inserts.

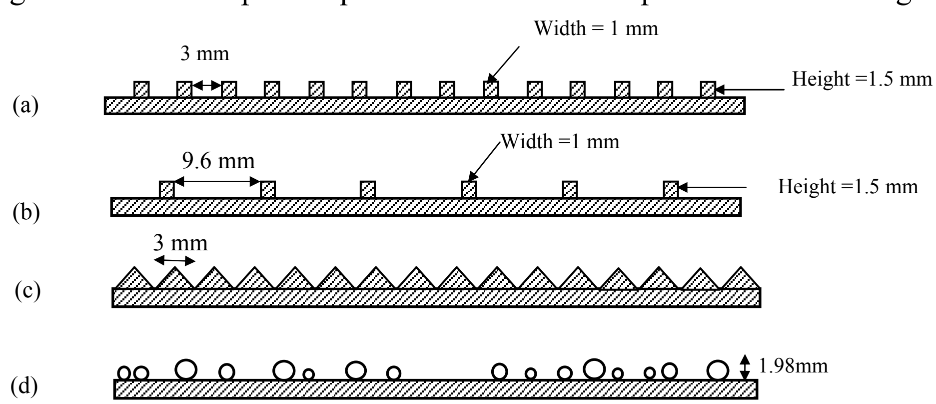

Figure 1. Side view of different types of 3D printed boundaries in CAD model (a) grid plate (R=1.5) (b) wide spaced grid (R=4.8) (c) saw tooth (ST) (d) fixed-particle (FX).

Before performing tests on the 3D printed boundary plates, 'verification tests' were conducted on dense Ottawa sand samples using metal grid inserts and 3D printed inserts with the same geometry (Figure 1a) to ensure that a similar response would be obtained by the 3D printed plates. The material stiffness and surface properties of the 3D printed plates differed from the typical metal plates used in the device and it was important to ensure that this did not affect the response. The verification tests compared the responses of dense sand samples under three initial vertical stresses of 50 kPa, 100kPa, and 150 kPa with a void ratio varying from 0.49 to 0.53. Two tests were conducted on each initial stress with one boundary condition and the results were averaged to improve the clarity of the stress-displacement response and vertical displacement. The tests were categorized according to the type of test (V-verification), initial normal stress, and boundary designation (R=1.5, R=4.8, ST- saw tooth, FX - fixed).

Following the verification experiments, only the 3D printed boundaries were used in the experiments on dense ball bearings under the initial normal stresses of 50 kPa, 100kPa, and 150 kPa with a void ratio varying from 0.53 to 0.62. This research used American Iron and Steel Institute (AISI) 52100 Grade 25 precision chrome steel spheres manufactured by Thompson Precision Ball. Due to the tendency of uniform sized spheres to crystallize (i.e., form regular packings), three different diameters of spheres were used (Table 1) in the experiments. The samples were comprised of approximately 8,862 particles of each of the three sizes, totaling approximately 26,586 particles.

Table 1. Properties of steel ball bearings used in direct shear experiments.

Property	Value
	1.98
Nominal diameter (mm)	1.59
	1.19
Density (kg/m^3)	7800
Shear modulus (GPa)	80
Poisson's ratio	0.3

Similar to the verification study, 2 experiments were conducted for each set of test conditions and the results were averaged to improve the clarity in the comparisons. Table 2 provides the full list of experiments conducted, as well as the corresponding test conditions.

Table 2. Details of direct shear experiments conducted on metal and 3D printed boundaries.

Test designation	Void ratio	Test designation	Void ratio
VM-50	0.52,0.53	R=4.8-50	0.55,0.54
VM-100	0.53,0.49	R=4.8-100	0.54,0.53
VM-150	0.52,0.53	R=4.8-150	0.55,0.55
V3D-50	0.52,0.52	ST-50	0.57,0.58
V3D-100	0.50,0.53	ST-100	0.58,0.58
V3D-150	0.52,0.52	ST-150	0.58,0.58
R = 1.5-50	0.57,0.57	FX-50	0.62,0.62
R=1.5-100	0.57,0.57	FX-100	0.62,0.62
R=1.5-150	0.57,0.57	FX-150	0.61,0.62

VERIFICATION RESULTS ON SAND SAMPLES WITH METAL AND 3D PRINTED GRID INSERTS

The results of the experimental tests conducted on dense Ottawa sand with the metal grid inserts and similar 3D printed grid inserts with R=1.5, under three different initial vertical stresses, are illustrated in Figure 2. At the initial vertical stresses of 50 kPa and 100 kPa, peak shear stresses, as well as the full stress responses for the metal grid inserts and the 3D printed grid inserts are approximately the same. However, at an initial vertical stress of 150 kPa, the post peak stress response shows a small amount of variation for the metal and the 3D printed grid plates. The vertical displacement (Figure 2b) of the sand on the two different grid plates also agrees quite well with no considerable variation observed. For 50 kPa, the dilation is slightly higher for the 3D printed grid inserts than regular metal grid inserts, but at higher stresses, the vertical displacement is very similar. Hence, the tests reinforce the observation that the boundary material type has little or no influence on contraction or dilation behavior and that the 3D printed inserts are sufficient for further use in the direct shear device.

The peak shear stresses at the tested normal stresses, as well as the angle of shearing resistance determined for the metal and the 3D grid inserts with R=1.5 are displayed in Figure 3. The values of the average angle of shearing resistance obtained for the metal grid plates and the 3D printed plates are 29.4° and 30.8°, respectively. These values indicate that there is no considerable difference in the response of sand for the metal and 3D printed boundary plates used in the current study. Overall, there is no significant difference in the stress-displacement or the vertical displacement responses of sand when grid inserts with the same geometry comprised of two different materials are used. Therefore, for the remainder of the study, only the 3D printed boundaries were used.

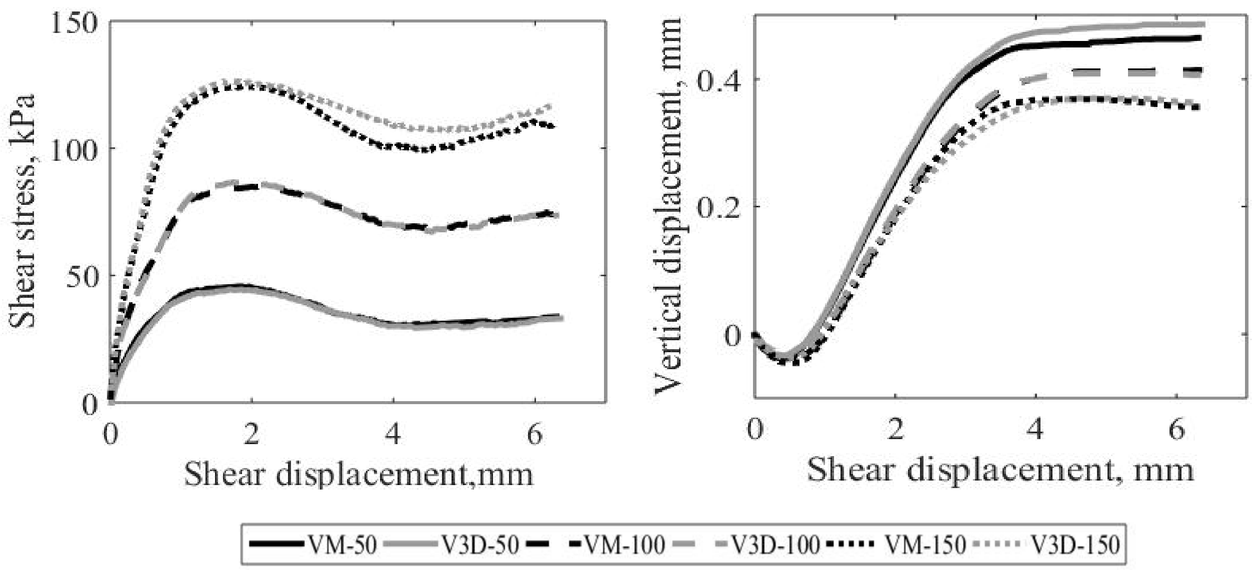

Figure 2. Results of sample configuration V (verification tests) at 50 kPa, 100 kPa and 150 kPa with R=1.5 metal (M) and 3D printed (3D) grid plates.

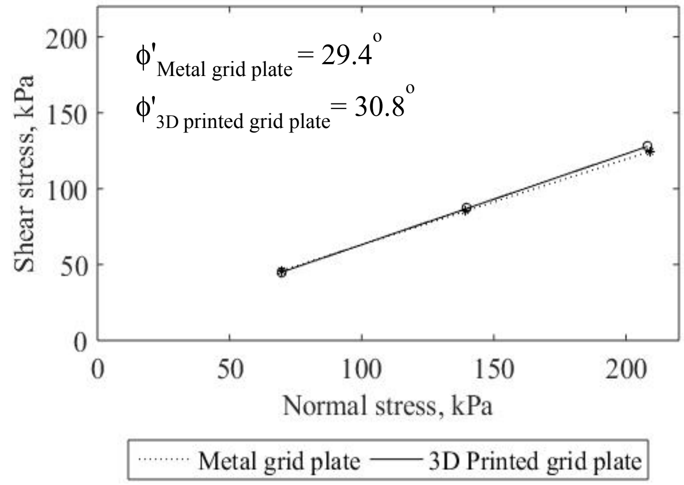

Figure 3. Comparison of peak shear stress at select normal stresses for verification tests with R=1.5 metal grid plates and 3D printed plates.

RESPONSE OF BALL BEARINGS WITH 3D PRINTED GRID INSERTS

The ball bearings were air pluviated into the direct shear box in three layers and then vibrated and tamped to make the dense samples. Depending on the type of the grid inserts used, the calculated void ratio varied slightly, although the samples were likely at very similar actual void ratios. The chrome steel metal ball bearings are very smooth and pack well, making it easy to replicate samples at the densest state with very little variation in void ratio. For example, for a given boundary type, replicate samples could be created at void ratios within 0.01 or 0.02 of one another. Overall for the four boundary types tested, the void ratios varied from 0.53-0.62, with the R=4.8 grid plate samples having the smallest void ratios and the fixed-particle boundary samples having the highest void ratios. While the volumes of the grid and sawtooth geometries were taken into account in the calculations, the differences in void ratios could be caused by slight measurement errors in the estimation of the volume occupied by the projected geometries. Also, the fixed-particle boundary had excess epoxy in some regions which was not considered in the calculations. Therefore, for the analysis below, it was assumed that the samples were actually at similar initial void ratios and that the differences observed were due to slight errors in the calculation of the total volume of the sample when taking into account the boundary insert geometries.

The stress and vertical displacements of the dense ball bearings with different boundaries tested under 50 kPa initial vertical stress are presented in Figure 4. The stress-displacement responses for the four different boundary types at 50 kPa are very similar; however, the vertical displacement differs for the samples. The initial contraction is the same for all samples, but the dilation at higher shear displacements becomes quite different for the sawtooth and fixed-particle boundary. The fixed-particle boundary tests resulted in the highest dilation, whereas the sawtooth boundary tests showed the lowest dilation. One thought was that the sawtooth geometry at the boundary of the samples might not have allowed a tight packing due to the size of the asperities in relation to the particle size. Additional tests were conducted making sure to check that the top cap was seated properly in the densest possible state. The dilation was also observed to be lower for these tests than what was observed for the other boundary types, indicating that the behavior was a result of the boundary geometry rather than a function of void ratio and the seating condition of the top cap.

For tests conducted at an initial normal stress of 100 kPa, the fixed-particle type boundary produced higher peak stresses, as shown in Figure 5. The two types of grid inserts resulted in similar stress-displacement behavior and approximately the same peak stress while the saw tooth plate led to a lower peak stress than all the other boundary types. The vertical displacement also showed some differences at higher shear displacements for the fixed-particle and sawtooth boundaries, although the fixed-particle boundary samples did not exhibit the greatest dilation. The vertical displacements of the two grid inserts were very similar, but overall they were higher than that of fixed boundary which differs from their behavior under an initial vertical stress of 50 kPa. The two grid plates had projections with the same height with the only differing factor being the spacing between projections. This data indicates that the grid spacing does not influence the behavior of the granular material if they are sufficiently large.

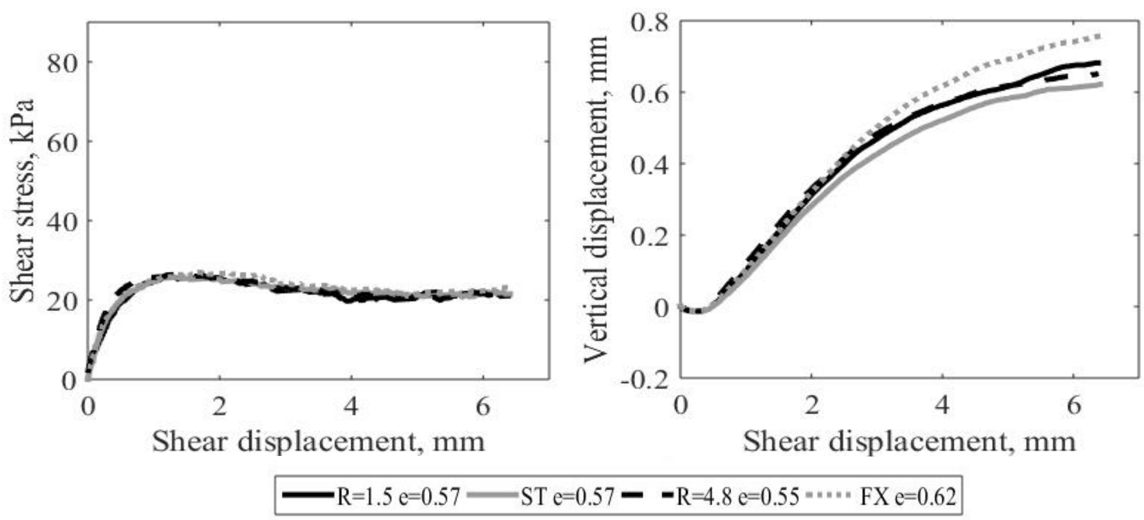

Figure 4. Results of sample configuration R,ST, and FX at 50 kPa vertical effective stress.

The stress-displacement and vertical displacement of samples at 150 kPa are illustrated in Figure 6. When tested under an initial vertical stress of 150 kPa, the saw tooth boundary produced the lowest peak stress, similar to results at 100 kPa. The grid insert responses were consistent with nearly superimposed stress-displacement curves. The fixed-particle boundary also showed a similar peak stress to that of the grid inserts. As for the vertical displacement of the particles, the fixed-particle boundary samples exhibited less dilation than the grid boundaries. At all three normal stresses tested, the samples with the sawtooth boundary dilated much less when compared to the other boundary types.

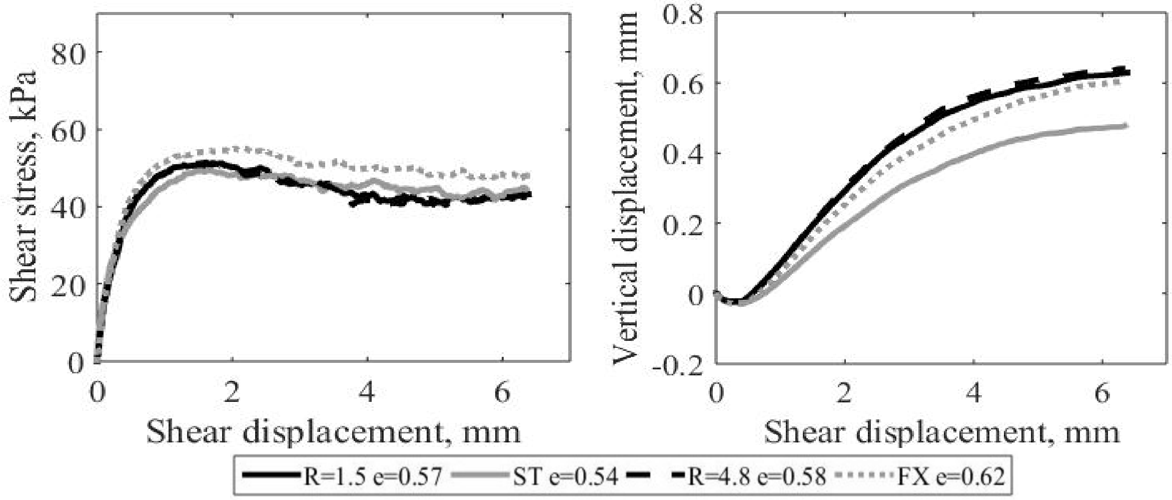

Figure 5. Results of sample configuration R,ST, and FX at 100 kPa vertical effective stress.

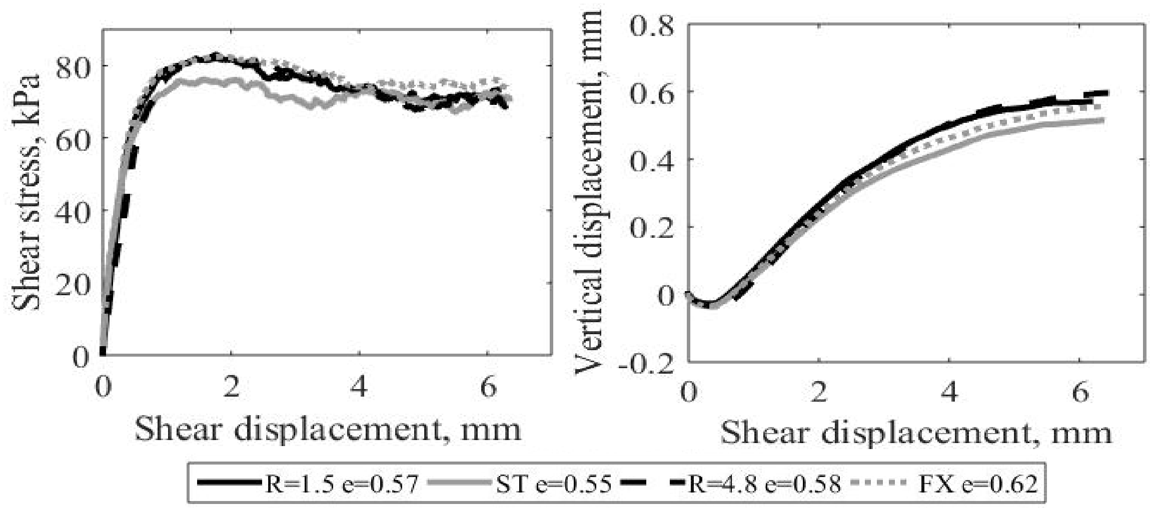

Figure 6. Results of sample configuration R,ST, and FX at 150 kPa vertical effective stress.

The angle of shearing resistance obtained from Figure 7, for the grid inserts with R = 1.5, grid inserts with R=4.8, saw tooth, and fixed-particle boundary tests are 23.4°, 23.1°, 20.8°, and 22.9°, respectively. While overall the results are somewhat similar, the friction angle obtained for the sawtooth plates is the lowest. This agrees with the fact that the sawtooth samples exhibited the lowest dilation of all the samples.

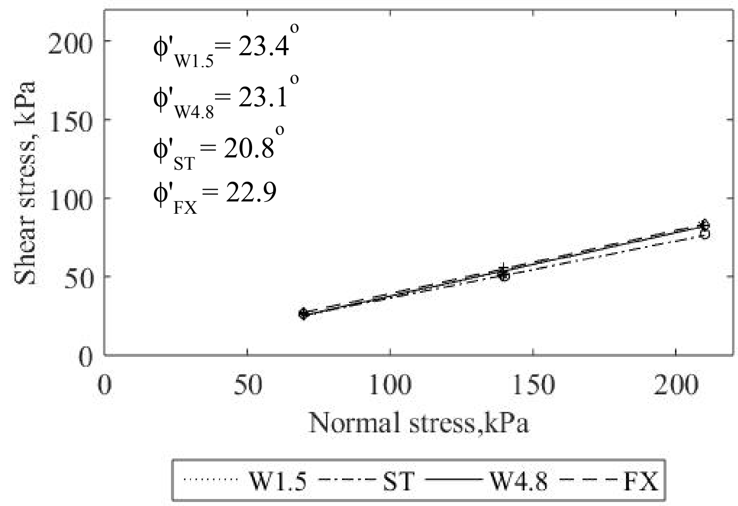

Figure 7. Friction angle of ball bearings with different 3D printed boundaries.

CONCLUSIONS

Four different types of boundaries for a direct shear device are examined to determine their effects on the stress-displacement and vertical displacement responses of granular materials. Verification tests were conducted on sand to compare typical metal grid inserts and 3D printed grid inserts. These tests showed no considerable differences in soil response. Therefore, additional direct shear tests were performed on precision ball bearings using four different 3D printed boundaries. The results indicate that the sawtooth boundary samples exhibit lower peak strength and less dilation at all stresses tested, although the difference is not as pronounced for tests conducted at a vertical stress of 50 kPa. Because the void ratios of the samples were likely very similar, this difference in response is attributed to the geometry of the plates. The spacing of the typical grid plate projections showed little influence on the response; however, only two spacings were tested. Future testing will consist of direct shear tests on loose samples of the metal ball bearings, as well as dense and loose samples of Ottawa sand to determine if boundary effects are seen for more angular soils or if density influences the responses. Finally, results from the direct shear tests on metal ball bearings will be used for experimental validation of DEM simulations of spherical particles under the same boundary and stress conditions.

REFERENCES

Bernhardt, M. L, Biscontin, G., and O' Sullivan, C. (2016). "Experimental validation study of 3D direct simple shear DEM simulations", *Soils and Foundations* 2016; 56(3):336–347.

Cui, L. and O'Sullivan, C. (2006). "Exploring the macro- and micro-scale response of an idealized granular material in the direct shear apparatus." *Geotechnique*, 56, 455-468.

Hryciw, R. D. and Irsyam, M. (1993). "Behavior of sand particles around rigid inclusions during shear", Soils and Foundations, Vol. 33, No. 3, 1-13.

O'Sullivan, C., (2011). "Particulate Discrete Element Modelling", CRC Press, London.

Uesugi, M., and Kishida, H (1986), "Influential Factors of Friction between Steel and Dry Sands," *Soils and Foundations*, 26(2), 33-46.
Yoshimi, Y and Koshida, T (1981), "Friction between sand and metal surface", Proceedings of 10^{th} ICSMFE, Vol. 1, 831-834.
ASTM D3080, (2012), "Standard Test Method for Direct Shear Test of Soils under Consolidated Drained Conditions1", ASTM International, West Conshohocken, PA.

Impact of Wet-Dry Cycles on the Shear Strength of High Plastic Clay Based on Direct Shear Testing

M. A. Khan[1]; M. S. Hossain[2]; M. S. Khan[3]; S. Samir[4]; and Al Aramoon[5]

[1] Graduate Research Assistant, Dept. of Civil Engineering, The Univ. of Texas at Arlington, 416 Yates Street, NH 119, TX 76019. E-mail: md.khan22@mavs.uta.edu
[2] Professor, Dept. of Civil Engineering, The Univ. of Texas at Arlington, 416 Yates Street, NH 119, TX 76019. E-mail: Hossain@uta.edu
[3] Assistant Professor, Dept. of Civil Engineering, Jackson State Univ., 1400,John R Lynch Street, Jackson, MS 39217. E -mail: j00797693@jsums.edu
[4] Manager, Solid Waste Institute for Sustainability, 417 Yates Street, NH 119, TX 76019, United States. E-mail: sonia.samir@ymail.com
[5] District Material Engineer, Dallas District, Texas Dept. of Transportation, 4777 E Highway 80, Mesquite, TX 75150-6643.

Abstract

Cyclic wetting and drying of compacted highly plasticity clays and shales cause volume change through shrinkage and swelling. This eventually may decrease the shear strength to the fully softened state. The objective of the current study is to determine the change in strength as well as physical properties of high plasticity clay due to repetitive swelling and shrinking over time. During this research, the effects of cyclic wetting and drying on the shear strength of the clayey soil were investigated. Soil samples were collected from a slope located on I 35 near Mockingbird, Dallas to prepare test specimens which were subjected to 1, 3, and 5 wet-dry cycle before the direct shear testing. It is observed that the angle of internal friction decreased by 6^{o} and cohesion decreased by 55% of initial compacted stage after the fifth wet-dry cycle.

INTRODUCTION

The slope failure and landslide causes significant hazards to public and private sectors. The cost associated with routine maintenance and repair of "surficial" slope failures is significant but generally neglected (Loehr and Bowders 2007). For compacted clay embankments, the main reason behind the decrease in shear strength appears to be weathering which will decrease the drained shear strength of compacted clays towards the fully softened shear strength (Castellanos et al. 2015).

Determination of soil strength parameters for shallow slope stability analysis is the most important task as the factor of safety will be significantly reduced (Rogers and Wright 1986) with the number of wetting and drying cycles. Wetting and drying (w-d) cycles reduce the expansive nature and increase the collapse tendency of the high plasticity clay (Alonso and Gens 1999; Zubaydi 2011). Many researchers, such as Wheeler et al. (2003), Alonso et al. (2005), have reported the behavior of expansive soils during wetting and drying cycles by controlling the suction. Some others have shown that behavior of expansive soil changes with chemical influence (Castellanos et al. 2008). Estabragh et al. (2013) have investigated the impact of wetting fluid on swelling potential. He also reported that deformation increased with the number of wetting and drying cycle and reached to equilibrium condition after the fifth cycle. Rogers and Wright (1986) also reported that wetting and drying can reduce the strength of high plastic clay which was reflected by the decrease of cohesion intercepts with only a minor change in friction angle. Reduction of soil strength due to weathering may reduce the factor of safety of a slope with time. According to the shallow slope failure mechanism (Lade 2010), the factor of safety should be calculated for infinite slope and seepage should be considered parallel to the slope surface.

The main objective of this research work is to determine the impact of wet dry cycle on the mechanical properties of high plastic clay which is very important for shallow slope stability analysis. Changes in basic soil properties such as moisture content and void ratio can provide an important insight about the change in soil strength parameters. To simulate the shallow slope failure condition, direct shear tests in the laboratory were conducted at low normal stresses with the soil samples that went through different numbers of wet-dry cycles. Void ratio, density, degree of saturation and moisture content were calculated from the identical soil samples prepared for each wet-dry cycle.

MATERIALS AND METHODS

Soil samples were collected from a slope located in Mockingbird, I 35 in Dallas, Texas. Collected soil samples from the bore holes were first broken down into small pieces and kept in the oven for 24 hrs. for drying. Oven dried soil was pulverized prior to grain size distribution analysis. Sample passing #40 sieve was used for the determination of liquid limit and plastic limit according to ASTM D4318. Samples having liquid limit more than 50 was separated and used for further investigations. Wet sieving method was used to separate the particles passing #200 sieve. Particle that retained on #200 sieve was used to determine the grain size distribution according to ASTM D422 and hydrometer analysis was used for the soil particle smaller than 0.075 mm. Water pycnometer was used to determine the specific gravity of soil using ASTM D854. For the preparation of test specimen, compaction was performed using the same energy level provided by a standard proctor test (ASTM D 698). Soil properties are shown in Table 1. The direct shear test apparatus (HM 2560A) used in this investigation had a pneumatic loading piston for applying the vertical load to the sample. This shear testing device has a large digital display for controlling load and displacement for both vertical and horizontal directions. Linear strain transducers were used to measure the vertical and shear displacements while vertical load was measured with a pressure transducer. A load cell was used to measure the load in horizontal direction. A 63.5 mm (2.5 inch) diameter shear box was used for testing with maximum possible shear displacement of 20 mm (0.8 in). It is possible to set the rate of shearing up to 0.025 mm/min

Table 1: Soil Properties

Physical Properties	**Values**
Unified Classification	CH
Maximum unit weight	18.15 KN/m^3 at 19%
Liquid Limit	80%
Plastic Limit	32%
Plasticity Index	48%
Percent of Clay	54%
Specific Gravity	2.72